International Journal of Structural Stability and Dynamics
Vol. 5, No. 3 (2005) 359–385

World Scientific
www.worldscientific.com

TRANSITIONS FROM REGULAR TO CHAOTIC VIBRATIONS OF SPHERICAL AND CONICAL AXIALLY-SYMMETRIC SHELLS

J. AWREJCEWICZ*, V. A. KRYSKO† and T. V. SHCHEKATUROVA‡

*Technical University of Lodz, Department of Automatics and Biomechanics
1/15 Stefanowskiego St., 90-924 Lodz, Poland
awrejcew@p.lodz.pl

†,‡Saratov State University, Department of Mathematics
410054, B. Sadovaya, 96 Saratov, Russia
‡tak@san.ru

Received 13 September 2004
Accepted 8 June 2005

By the variational principle, the chaotic vibrations of deterministic geometrically nonlinear elastic spherical and conical axially symmetric shells with non-homogeneous thickness subjected to a transversal harmonic load are analyzed. The material of the shells is assumed to be isotropic and of the Hookean type. Inertial forces tangent to the averaged surface and inertia of rotation of the cross-section are neglected. By the Ritz procedure, the original PDEs are transferred to the ODEs (Cauchy problem), which are then solved by the fourth-order Runge–Kutta method. In the numerical studies, scenarios of transitions from harmonic to chaotic states for vibrations of flexible spherical and conical shells are detected. Various vibrational states for different combinations of the following control parameters: shell's deflection arrow, the amplitude and frequency of the exciting force, number of modes considered, boundary conditions, and the thickness and shape of the shell cross-section are studied. By adjusting the above parameters, we can detect the transition of a continuous system to the lumped one, and the transition from the harmonic to chaotic vibrations.

Keywords: Ritz method; shells; chaos; ordinary and partial differential equations.

1. Historical Introduction

The variational methods play a key role in the formulation of dynamic problems for shells. Beginning from the pioneering work of Ritz[1] who, in 1908, proposed the minimization of a series of functions, a new challenging area of applications in applied mechanics has been opened. Many difficult problems have been solved successfully by the Ritz method. Other researchers, particularly Timoshenko, developed and applied this method to various problems of applied sciences and engineering. Methods of Ritz and Bubnov–Galerkin require essentially smaller numbers of operation in comparison with the other methods. They require less computational time, and in some cases allow the analytical solution to be obtained.

The stability of the Ritz process is an important issue. For instance, Mikhlin[2,3] has shown that for linear stationary processes, the stability of the Ritz procedure is determined by certain properties of coordinate elements, whereas Dovbysh[4,5] has analyzed the stability of the Ritz process in various spectral problems.

In the field of nonlinear problems the following problems have been successfully solved. The nonlinear stationary problem of shells governed by the hybrid type equations has been solved by the Ritz process by Kantor.[6] Various forms of variational equations have been formulated from the variational principle through the use of different variational functions (see for instance the works of Ainola,[7] Galimov,[8] Mushtari and Galimov,[9] Reissner[10]).

One application of the variational methods is associated with the proof of existence and the formulation of solutions for nonlinear problems of elasticity and plasticity. Here, the works of Vorovich[11] for the nonlinear theory of shells should be mentioned, in which the original problem is reduced to the solution of the system equations with the nonlinear and continuous operators reserved. Applying the topological methods, Vorovich proved the compactness of the approximate solutions obtained by Ritz's method. In addition, he proved that each of the points of the Ritz manifold corresponds to one solution of the Cauchy problem. The series of theorems, proved by Vorovich,[11] give an estimation of the approximate solution to the stationary problems.

By the Ritz approach, an equation of the hybrid form can be derived with respect to the deflection and stress functions. This equation is associated with the variational principle situated between Lagrange and Castigliano principles, where displacements and stresses are variated in a mean surface. A peculiarity of this equation is exhibited by a functional standing under the variational sign. Namely, this functional is not equal to the total energy of the system, although a variation of this functional coincides with that of the total energy.

Usually, four different approaches are adopted for searching the solution of a stationary nonlinear Ritz system:

1. the Newton–Kantorovich method,
2. method of differentiation with respect to the parameter,
3. method of successive approximations,
4. "set-up method" proposed firstly by Fedos'ev[12] and widely applied in works.[13,20]

It has been shown in Ref. 5 that differentiation with respect to the parameter and the Cauchy problem for ODEs with independent variable t should be solved on the fixed time interval $0 \leq t \leq 1$, if the initial system behaves as the Ritz system for a certain functional. The aforementioned functional should posses a polynomial increase up to infinity. For this case, an identity of the Ritz and Bubnov–Galerkin processes is established.

To the knowledge of the authors, an appropriate numerical solution to the chaotic processes of the deterministic systems represented by spherical and shallow shells with homogeneous and non-homogeneous thickness has not been made

available. The aim of this work is to fulfil such a gap. It is noted that for spherical shallow shells, rectangular plates, and plates of infinite length subjected to longitudinal sinusoidal loadings, similar approaches have been presented in Refs. 13–21.

2. Ritz Method

Consider a double-curvature shallow shell in a three-dimensional space R^3 with a curvilinear system of coordinates α, β, γ, as shown in Fig. 1, in which $\gamma = 0$ denotes the mean surface. The axes $o\alpha$ and $o\beta$ are directed along the main curves of the two curvatures associated with the surface, whereas the axis $o\gamma$ is oriented toward the center of the curvatures. With the given coordinates, the shell is defined as a 3D object as $\Omega = \{\alpha, \beta, \gamma / (\alpha, \beta) \in [0, a] \times [0, b], -\frac{h}{2} \leq \gamma \leq \frac{h}{2}\}$.

It is assumed that the function $h(\alpha, \beta)$ does not possess first-order discontinuities, and the maximal thickness $h_{\max} \equiv h_0$ is much smaller than the main curvature radius $R_{\min}$. It is also assumed that the Kirchhoff–Love hypothesis for normal coordinates holds. By the principle of virtual displacements, one gets

$$-\delta(U_u + U_c) + \iint R\delta w \, ds = 0. \tag{1}$$

The first term of Eq. (1) represents the virtual work of elastic forces acting on the shell, and the second term the virtual work due to the applied loads and D'Alembert and dissipative forces of the form

$$R = q - \frac{h\gamma_*}{g}(\ddot{w} + \varepsilon \dot{w}), \tag{2}$$

where γ_* is the unit weight, g the gravitational acceleration, q the transversal load, ε the coefficient of dissipation, and h the thickness of the shell.

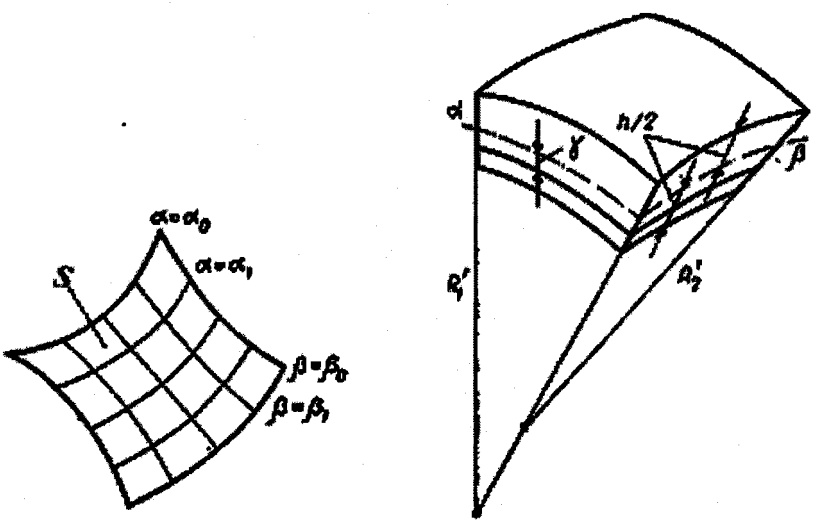

Fig. 1. The geometry and mean surface of the shell.

Notice that in Eq. (1), δU_u is the variation of the potential energy, caused by bending deformations of the form

$$\delta U_u = \iint (M_1 \delta\chi_1 + M_2 \delta\chi_2 + 2M_{12}\delta\chi_{12}) ds, \tag{3}$$

where M_1, M_2, M_{12} are the bending and rotational moments, $\chi_1, \chi_2, \chi_{12}$ are parameters describing the curvature changes of the mean shell surface, and δU_c is the energy variation, associated with the deformation of the mean surface:

$$\begin{aligned}\delta U_c &= \iint (T_1 \delta\varepsilon_1 + T_2 \delta\varepsilon_2 + T_{12}\delta\varepsilon_{12}) ds \\ &= \delta \iint (T_1\varepsilon_1 + T_2\varepsilon_2 + T_{12}\varepsilon_{12}) ds - \iint (\varepsilon_1 \delta T_1 + \varepsilon_2 \delta T_2 + \varepsilon_{12}\delta T_{12}) ds,\end{aligned} \tag{4}$$

where $T_1, T_2, T_{12}, \varepsilon_1, \varepsilon_2, \varepsilon_{12}$ are, respectively, the stresses and deformations occurring in the mean surface.

Since the hypothesis of straight normals holds, the strains at an arbitrary point of the shell have the following form:

$$\begin{aligned} e_1 &= \varepsilon_1 + \gamma\chi_1, \\ e_2 &= \varepsilon_2 + \gamma\chi_2, \\ e_{12} &= \varepsilon_{12} + 2\gamma\chi_{12}, \end{aligned} \tag{5}$$

where the strains at the mean surface are given as

$$\begin{aligned} \varepsilon_1 &= \frac{\partial u}{\partial\alpha} + \frac{1}{2}\left(\frac{\partial w_1}{\partial\alpha}\right)^2 - \frac{1}{2}\left(\frac{\partial w_0}{\partial\alpha}\right), \\ \varepsilon_2 &= \frac{\partial v}{\partial\beta} + \frac{1}{2}\left(\frac{\partial w_1}{\partial\beta}\right)^2 - \frac{1}{2}\left(\frac{\partial w_0}{\partial\alpha}\right), \\ \varepsilon_{12} &= \frac{\partial u}{\partial\beta} + \frac{\partial v}{\partial\alpha} + \frac{\partial w_1}{\partial\alpha}\frac{\partial w_1}{\partial\beta} - \frac{\partial w_0}{\partial\alpha}\frac{\partial w_0}{\partial\beta}, \\ w_1 &= w + w_0. \end{aligned} \tag{6}$$

In the above, u, v describe the displacements in the direction of α and β, respectively. $w(w_0)$ is the initial deflection. Notice that in Eq. (6) the quadratic terms relate to the geometrical nonlinearity associated with the normal rotation (with respect to the mean surface) resulting from extensions and rotations. Equation (6) can be derived from more generalized formulas.[22]

It should be noted that Eq. (6) is approximate in nature even for the linear part. In exact formulas (see Eq. (12.53) in Ref. 23) the terms u/R_1 and v/R_2, where R_1 and R_2 are the main radii, are also included. Neglecting these terms is one of the assumptions of the technical theory of shells adopted in this work. For the case of plates or for the case with axially symmetric deformation ($v \equiv 0$), such as cylindrical and shallow shells ($R_1 \equiv \infty$), the aforementioned terms also reduce to zero. The parameters characterizing the changes in the mean curvature are

$$\chi_1 = -\frac{\partial^2 w}{\partial\alpha^2}, \quad \chi_2 = -\frac{\partial^2 w}{\partial\beta^2}, \quad \chi_{12} = -\frac{\partial^2 w}{\partial\alpha\partial\beta}. \tag{7}$$

The relations between the stresses and strains are

$$\begin{aligned}\sigma_1 &= \frac{E}{1-\nu^2}[\varepsilon_1 + \nu\varepsilon_2 + \gamma(\chi_1 + \nu\chi_2)]\\ \sigma_1 &= \frac{E}{1-\nu^2}[\varepsilon_2 + \nu\varepsilon_1 + \gamma(\chi_2 + \nu\chi_1)]\\ \sigma_{12} &= \frac{E}{2(1+\nu)}(\varepsilon_{11} + 2\gamma\chi_{12})\end{aligned} \tag{8}$$

where E is the elasticity modulus, and ν Poisson's ratio.

Integrating Eq. (8) with respect to the thickness, one gets the expressions for forces. By multiplying Eq. (8) by γ and integrating over the cross-section, one obtains the expressions for moments. Having the stresses, one can compute the deformations in the mean surface, which are required for expressing the functional in a hybrid form. By substituting the expressions for the strains in the mean surface, making use of the expressions in Eqs. (3) and (4), one can derive from Eq. (1) the following variational equation:

$$\delta \iint_S \left\{ \frac{D}{2}[(\Delta w)^2 - (1-\nu)L_2(w,w)] - \left[\Delta_k \varphi + L_2\left(\frac{1}{2}w + w_0, \varphi\right)\right] w \right.$$
$$\left. - \frac{1}{2Eh}[(\Delta\varphi)^2 - (1+\nu)L_2(\varphi,\varphi)] \right\} ds - \iint_S \left[q - \frac{h\gamma_*}{g}(\ddot{w} + \varepsilon\dot{w})\right] \delta w \, ds = 0 \tag{9}$$

where D denotes the cylindrical stiffness; $\Delta(\bullet)$ the Laplace operator; w, φ the deflection and stress functions, respectively; w_0 the initial deflection; and $L_2(\bullet)$ the known nonlinear operator for the theory of flexible shells.

The Ritz method cannot be directly applied to solving Eq. (9), where the deflection function w and stress function φ can be independently varied, since this equation does not have the form of functional variations (in fact they are equal to zero). In order to find the approximate values of the elements w^0 and φ^0, the coordinate series $w_i(\alpha,\beta)$ and $\varphi_i(\alpha,\beta)$ $(i = 1, 2, 3, \ldots)$ are applied. They should satisfy the following four requirements:

1. $w_i \in H_A, \varphi_i \in H_A$, where H_A is the Hilbert space referred to as the energy space;
2. $\forall i$ elements w_i and φ_i are linearly independent;
3. the system of elements w_i and φ_i is full (compact) in H_A;
4. the system of elements w_i and φ_i satisfies the main boundary conditions.

The approximate solution is sought in the following form

$$w = \sum_{i=1}^{n} x_i(t) w_i(\alpha,\beta), \quad \varphi = \sum_{i=1}^{n} y_i(t)\varphi_i(\alpha,\beta). \tag{10}$$

The coefficients $x_i(t)$ and $y_i(t)$ are the desirable functions of time. By substituting Eq. (10) into (9), carrying out the variational operation and comparing the coefficients standing by δx_i and δy_i, the following system of equations is

obtained

$$\mathbf{A}(\ddot{\mathbf{X}}+\varepsilon\dot{\mathbf{X}})+\mathbf{B}\mathbf{X}+\mathbf{C}\mathbf{Y}+\mathbf{D}\mathbf{X}\mathbf{Y}=\mathbf{Q}q_0$$
$$\mathbf{C}\mathbf{X}+\mathbf{E}\mathbf{Y}+\frac{1}{2}\mathbf{D}\mathbf{X}\mathbf{X}=0 \tag{11}$$

where the following non-dimensional quantities are introduced: $t=\bar{t}\tau, \varepsilon=\bar{\varepsilon}/\tau$, with $\tau=\frac{a}{h_0}\sqrt{\frac{a^2\gamma_*}{Eg}}$ (a-shell radius), the loading parameter $q_0(t)=q(t)a^4/Eh_0^4$, $\bar{w}=\frac{w}{h_0}$, $\bar{x}_i=\frac{x_i}{h_0}$, $\bar{\varphi}=\frac{\varphi}{Eh_0^3}$, $\bar{y}_i=\frac{y_i}{Eh_0^3}$, $\bar{h}=\frac{h(\rho)}{h_0}$, with $h(\rho)=h_0(1+c\rho)$, $\rho=r/a$. Notice that for simplicity the bars were omitted in Eq. (11).

For shallow rotational shells with axially symmetric deformations and thickness $h=h_0(1+c\rho)$, the deflection w and stress function φ have the form

$$w=\sum_{i=1}^{n}x_i(t)w_i(\rho), \quad \varphi=\sum_{i=1}^{n}y_i(t)\varphi_i(\rho), \tag{12}$$

where the matrix coefficients occurring in Eq. (11) have the form

$$\begin{aligned}
A_{ik}&=\int_0^1(1+c\rho)w_iw_k\rho\,d\rho; \quad C_{ip}=-\int_0^1[\Delta_k\varphi_p+L_2(w_0,\varphi_p)]w_i\rho\,d\rho;\\
B_{ik}&=\frac{1}{12(1-\nu^2)}\int_0^1(1+c\rho)^3[\Delta w_i\Delta w_k-(1-\nu)L_2(w_i,w_k)]\rho\,d\rho\\
Q_i&=\int_0^1 w_i\rho\,d\rho;\\
D_{ikp}&=-\int_0^1 w_iL_2(w_k,w_p)\rho\,d\rho;\\
E_{jp}&=-\int_0^1\frac{1}{1+c\rho}[\Delta\varphi_j\Delta\varphi_p-(1+\nu)L_2(\varphi_j,\varphi_p)]\rho\,d\rho.
\end{aligned} \tag{13}$$

Solving the second equation of the system equations in Eq. (11) with respect to $\mathbf{Y}$ yields

$$\mathbf{Y}=\left[\mathbf{E}^{-1}\mathbf{C}+\frac{1}{2}\dot{(}\mathbf{E}^{-1}\mathbf{D}\mathbf{X})\right]\mathbf{X}. \tag{14}$$

After multiplying the first equation of Eq. (11) by $\mathbf{A}^{-1}$ and denoting $\dot{\mathbf{X}}=\mathbf{R}$, the equation can be reduced to the first order Cauchy problem of the form:

$$\begin{aligned}
\dot{\mathbf{R}}&=-\bar{\varepsilon}\mathbf{R}+[\mathbf{A}^{-1}\mathbf{C}+(\mathbf{A}^{-1}\mathbf{D}\mathbf{X})]\cdot\mathbf{Y}-\mathbf{A}^{-1}\mathbf{B}\mathbf{X}+q_0(\bar{t})\mathbf{A}^{-1}\mathbf{Q},\\
\dot{\mathbf{X}}&=\mathbf{R}.
\end{aligned} \tag{15}$$

The transformation is possible since the matrices $\mathbf{A}^{-1}$ and $\mathbf{E}^{-1}$ do exist, if the coordinate functions are linearly independent. Equations (15) can be solved by the fourth-order Runge–Kutta method with the following initial conditions:

$$x_i=0, \quad \dot{x}_i=0 \qquad \text{for } t=0.$$

Table 1. Approximate functions for different boundary conditions.

	$w_i(\rho)$	
$\varphi_j(\rho)$	$(1-\rho^2)^{i+1}$	$(1-\rho^2)^i$
ρ^{2j}	Unmovable clamping	Unmovable ball-type support
$(1-\rho^2)^{j+1}$	Movable clamping	Movable ball-type support

The approximate functions for four types of the boundary conditions are listed in Table 1.

In order to study the vibration of shallow conical shells, the shell is treated as a plate with initial deflection $w_0 = -k(1-\bar{\rho})$, ($k = H/h_o$ is the arrow deflection). For the four types of boundary conditions, the coefficients of the system in Eq. (15) are given as follows:

1. Unmovable clamping

$$
\begin{aligned}
A_{ik}^{(1)} &= \frac{1}{6+2i+2k} + c\frac{(4+2i+2k)!!}{(7+2i+2k)!!}, \\
B_{ik}^{(1)} &= \frac{4(i+1)(k+1)}{3(1-\nu^2)}\left\{\frac{1}{i+k+1}\left\{\frac{ik}{(i+k)(i+k+1)}\right.\right. \\
&\quad + \frac{3c^2}{2(i+k+2)}\left[\frac{6ik}{(i+k)(i+k-1)} - \frac{1+\nu}{2}\right]\Bigg\} \\
&\quad \left.\left. + \frac{3c(2i+2k-4)!!}{(2i+2k+3)!!}[15ik - (1+\nu)(i+k)(i+k-1)]\right\}, \qquad (16) \\
C_{ip}^{(1)} &= -2(p+1)\cdot\frac{H}{h_0}\left(-\int_0^1 (1-\rho^2)^{i+p+1}d\rho + 2p\int_0^1 \rho^2(1-\rho^2)^{i+p}d\rho\right), \\
E_{jp}^{(1)} &= 4ip[(j+p-1)(1+\nu) - 2jp]\left(\frac{1}{j+p-1} - \frac{c}{j+p-1/2} + \frac{c^2}{j+p}\right), \\
D_{ikp}^{(1)} &= 4(i+1)(k+1)p\frac{p!}{(i+k+1)...(i+k+p+1)}, \quad Q_i = \frac{1}{2(i+2)}.
\end{aligned}
$$

2. Movable clamping

$$
\begin{aligned}
A_{ik}^{(2)} &= A_{ik}^{(1)}, \quad B_{ik}^{(2)} = B_{ik}^{(1)}, \\
C_{ip}^{(2)} &= 2\frac{H}{h_0}\cdot p(2p-1)\cdot\int_0^1 \rho^{2p-2}\cdot(1-\rho^2)^{i+1}d\rho, \quad Q_i^{(2)} = Q_i^{(1)}, \\
E_{jp}^{(2)} &= -16(j+1)(p+1)\left\{\frac{pj}{(j+p+1)(j+p)(j+p-1)}\right. \\
&\quad + \frac{c^2}{2(j+p+1)(j+p+2)} \qquad (17) \\
&\quad \left.\times\left[\frac{6jp}{(j+p)(j+p-1)} - \frac{1-\nu}{2}\right]\right.
\end{aligned}
$$

$$- c\frac{(2j+2p-4)!!}{(2j+2p+3)!!}[15jp-(1-\nu)(j+p)(j+p-1)]\Bigg\},$$

$$D^{(2)}_{ikp} = -\frac{4(i+1)(k+1)(p+1)}{(i+k+p+1)(i+k+p+2)}.$$

3. Unmovable ball-type support

$$A^{(3)}_{ik} = A^{(1)}_{i-1,k-1},$$

$$B^{(3)}_{ik} = \begin{cases} \dfrac{2+c(4+3c)}{6(1-\nu)}, & k=i=1, \\ -\dfrac{c(4+5c)}{15(1-\nu)}, & i=1,\ k=2;\ i=2,\ k=1, \\ B^{(1)}_{i-1,k-1}, \end{cases}$$

$$C^{(3)}_{ip} = C^{(1)}_{i-1,p}, \quad D^{(3)}_{ikp} = D^{(1)}_{i-1,k-1,p}, \quad Q^{(3)}_{i} = Q^{(1)}_{i-1}, \quad E^{(3)}_{jp} = E^{(1)}_{jp}. \tag{18}$$

4. Movable ball-type support

$$\begin{aligned} &A^{(4)}_{ik} = A^{(1)}_{i-1,k-1}, \quad B^{(4)}_{ik} = B^{(3)}_{ik}, \quad C^{(4)}_{ip} = C^{(2)}_{i-1,p}, \\ &D^{(4)}_{ikp} = D^{(21)}_{i-1,k-1,p}, \quad Q^{(4)}_{i} = Q^{(1)}_{i-1}, \quad E^{(4)}_{jp} = E^{(2)}_{jp}. \end{aligned} \tag{19}$$

Note that in Eqs. (17)–(19) the doubled factorial is computed in the following way: $2n!! = 2\cdot 4\cdot 6\cdot\cdots\cdot 2n$; $(2n+1)!! = 1\cdot 3\cdot 5\cdot\cdots\cdot(2n+1)$.

3. Reliability of the Results Obtained

The proposed Ritz algorithm allows us to solve a wide class of both static and dynamic problems. Solutions to statical problems are realized through the "set-up" method by Fedos'ev.[12,34] According to the solution of the Cauchy problem for $\varepsilon = \varepsilon_{cr}$ for a series of transversal contact loads uniformly distributed on the shell surface, one obtains $\{q_i\} \to \{w_i, \varphi_i\}$, which yields a construction of dependencies $q[w(0)]$ and allows us to investigate the stress–strain state. The reliability of the results obtained and the solution efficiency are verified through comparison with results obtained by the Ritz method applied to various static problems for high order approximations $(m = n = 3)$.[6,24]

Let us apply the proposed approach to the spherical shell with $k = 5$ and moving clamping (Table 1). According to the "set-up" method, a stationary problem is reduced to the hybrid hyperbolic problem as given in Eq. (15), and the parabolic one. The latter is obtained from Eq. (15) by removing the second derivative in time to yield

$$\dot{\mathbf{X}} = \frac{1}{\varepsilon}\cdot\Bigg(\Big[\mathbf{A}^{-1}\mathbf{C} + (\mathbf{A}^{-1}\mathbf{D}\mathbf{X})\Big]\cdot\Big[E^{-1}\mathbf{C} + \frac{1}{2}(E^{-1}\mathbf{D}\mathbf{X})\Big] \cdot\mathbf{X} - \mathbf{A}^{-1}\mathbf{B}\mathbf{X} + q_0(\bar{t})\mathbf{A}^{-1}\mathbf{Q}\Bigg). \tag{20}$$

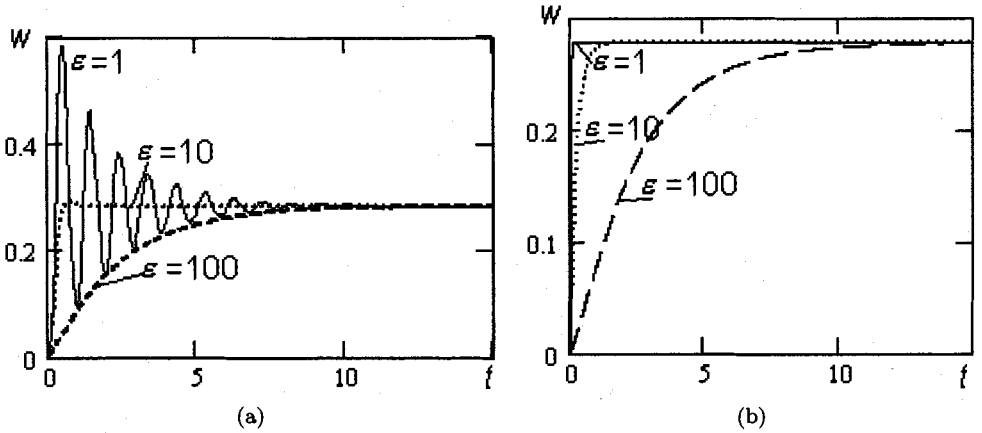

Fig. 2. Shell deflection for (a) hyperbolic, and (b) parabolic equations.

Table 2. Number of iterations.

ε	Hyperbolic Problem	Parabolic Problem
1	5096	50
10	512	492
100	5097	4929

The results obtained by the "set-up" method for the hyperbolic problem in Eq. (15) and parabolic problem in Eq. (20) for $\varepsilon = 1, 10, 100$ are plotted in Fig. 2.

The number of iterations required for obtaining the solution with a relative error $\varepsilon = 10^{-5}$ is shown in Table 2. It should be emphasized that the magnitude of ε essentially influences the number of iterations and the character of their convergence.

For the parabolic (hyperbolic) system, $\varepsilon = 1$ ($\varepsilon = 10$) is the optimal value for the computational procedure. However, the number of iterations needed for a hyperbolic problem is one order higher than that for a parabolic one. Hence, one may conclude that the so-called parabolic set-up method is more suitable for the case considered.

4. Convergence of the Ritz Method vs Control Parameters

In order to observe the qualitative behavior of the continuous system, a phase-space monitoring technique is employed. By this approach, the PDEs governing the dynamics of the continuous system are replaced by ODEs with infinite dimensions. However, some crucial points concerning such a reduction should be made here. First of all, instead of using an infinite chain of equations, one takes only its truncated version. It is realized that increasing the number of equations yields the threshold value, and further increase in the number of equations does not bring anything new, as the dynamical properties of the system have been stabilized. Obviously, such a reduction depends strongly on the finite dimension of the attractor analyzed. However, even for the finite dimension of the attractor, the truncation

procedure of Eqs. (10) and (12) plays an important role. It is worth noticing that for the case using an "improper" basis as the reduction tool to obtain the ODEs, the "truncated system" obtained may exhibit attractors with properties not comparable with those of the original system.

One example is the analysis of a two-dimensional equation governing the heat fluid convection. The Lorenz system,[25] as the "truncated" one, exhibits chaotic dynamics. However, an increase in the number of modes causes a non-regular increase in the chaos space, which then suddenly decreases. For a sufficiently large number of modes, chaos vanishes. It was shown in Ref. 26 that for large Prandtl numbers δ in the two-dimensional Boussinesque convection, there exist critical Rayleigh numbers Ra corresponding to the occurrence of one- and two-dimensional vibrating motions. A further increase of Ra pushes the system to harmonic convection. Both of the above examples show that in order to get qualitatively proper correspondences between the dynamics of the original and truncated dynamical systems obtained either by the Bubnov–Glaerkin or Ritz methods, one has to include an appropriate number of modes. This problem was addressed in consideration of the parametric vibrations for flexible plates in Ref. 27.

In what follows, we investigate the problem of an appropriate choice of the modes in the Ritz procedure using the example of vibrations of spherical and conical shallow and geometrically nonlinear shells with homogeneous and non-homogeneous thickness, and movably clamped on their contours. We assume the load to be uniformly distributed along the shell surface due to the harmonic rule of the form

$$q = q_0 \sin \omega_p t. \tag{21}$$

For the present purposes, the vibrations computed for a conical shell simply ball-type supported on its contour with different values of the control parameters $\{q_0, \omega_p\}$ have been plotted in Figs. 3(a) and 3(b) for $k = 5$ with constant and non-constant thickness ($h = h_0(1+c\rho)$) for $c = 0.1$, from which the convergence property of the Ritz procedure related to the shell thickness can be analyzed, as given below.

Consider point $A(q_0 = 2.4,\ \omega_p = 3.5) \in \{q_0, \omega_p\}$ in Fig. 3(a) which, for $n = 6$, is situated within a chaotic zone. In Fig. 4, the signals $w(0;t)$ for $150 \leq t \leq 156$ and power spectra $S(\omega_p)$ were plotted. Observe that for $n = 2$ harmonic vibrations with frequency ω_p, $n = 3$ show first the period doubling bifurcation; for $n = 1$, 4, 5, 6 chaos appears on the fundamental frequency. From these results, one concludes that beginning with $n \geq 4$ the bifurcational process for $k \leq 5$ is described properly, i.e. there is a convergent sequence,

$$\left[w^0 - \sum_{i=1}^{n} x_i(t) w_i(\rho)\right] = \min_{t \in [50,53]}$$

$$\left[\varphi^0 - \sum_{i=1}^{n} y_i(t) w_i(\rho)\right] = \min_{t \in [50,53]}$$

and it is the best approximation to the exact solution w^0 and φ^0 in the metric H_A.

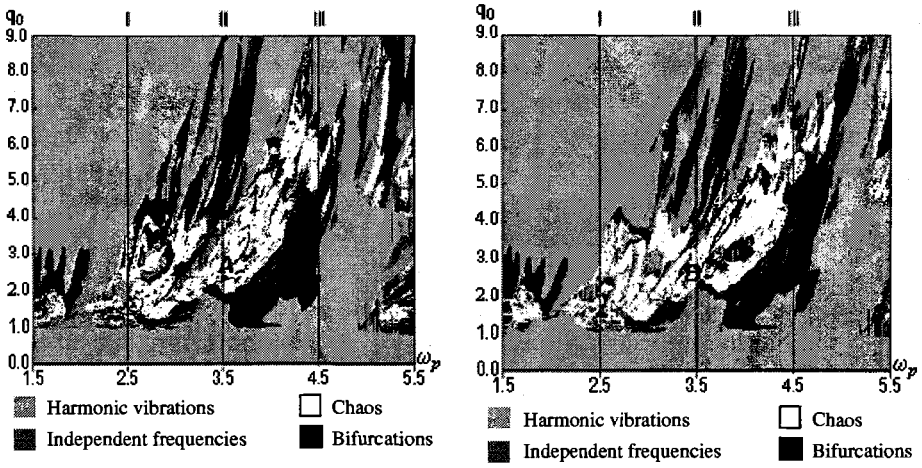

Fig. 3. Vibrations in terms of the control parameters $\{q_0, \omega_p\}$ for conical shell for $k = 5$ with (a) constant, (b) non-constant thickness.

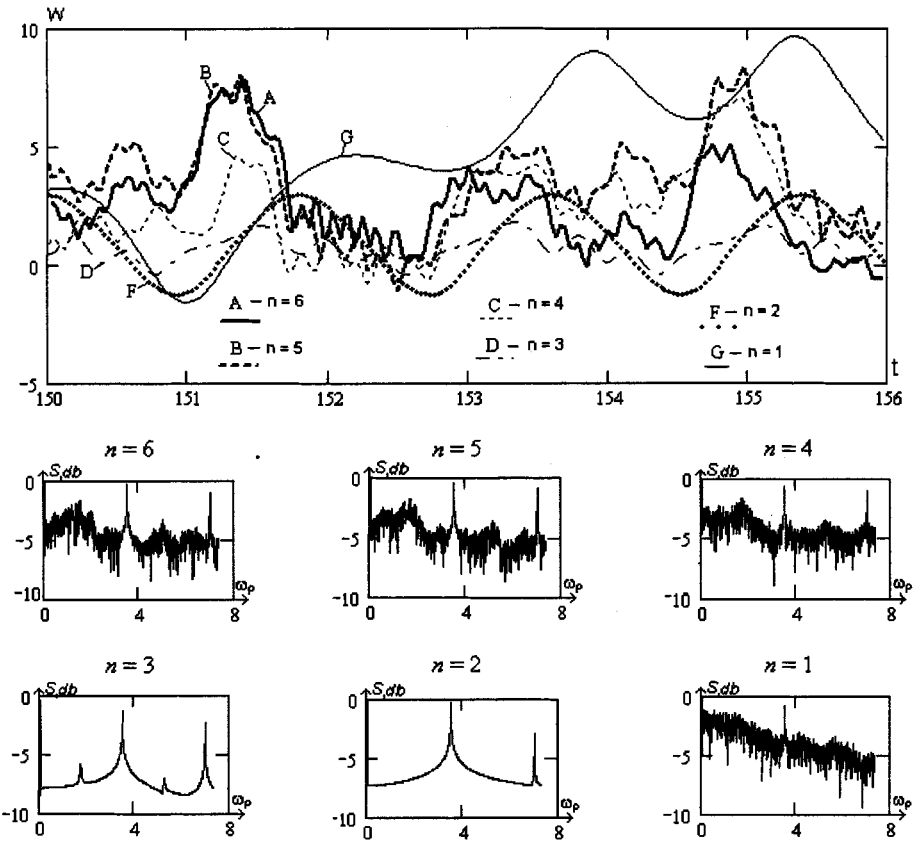

Fig. 4. Dependencies $w(0,t), t \in [150; 156]$ and $S(\omega_p)$ vs n in (12) for conical shell with constant thickness ($k = 5$) and movable simple ball-type support (constant thickness of the shell).

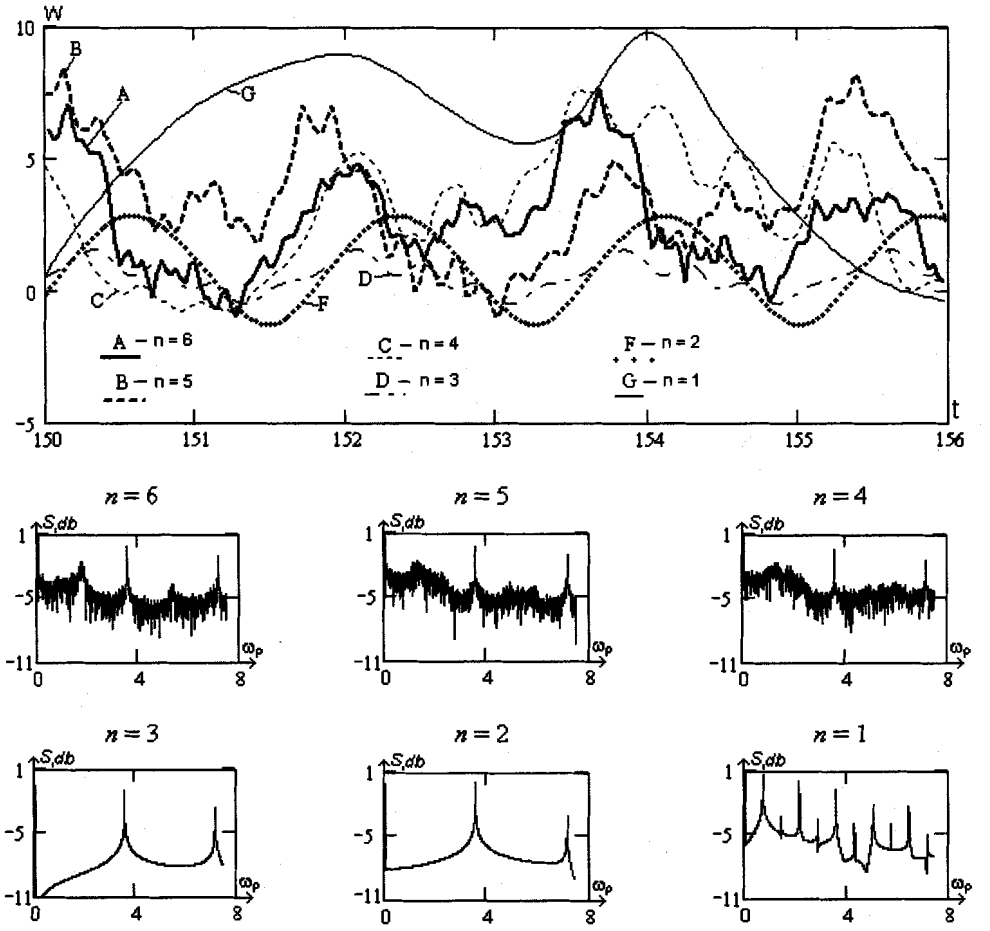

Fig. 5. Dependence $w(0,t), t \in [150;156]$ and $S(\omega_p)$ vs n in (12) for conical shell with constant thickness ($k = 5$) and movable simple ball-type support (non-constant thickness of the shell).

Consider now a shell with non-homogeneous thickness. Let us take the point $B(q_0 = 2.4,\ \omega_p = 3.57) \in \{q_0, \omega_p\}$ in Fig. 3(b) which, for $n = 6$, is situated in a chaotic zone. In Fig. 5 the following signals are reported: $w(0;t)$ for $150 \leq t \leq 156$ and a power spectrum. For $n = 2$ and $n = 3$ harmonic vibrations with the exciting frequency ω_p occur, whereas $n = 1$ corresponds to harmonic vibrations with the frequency of $1/5\ \omega_p$, which means that the first approximation in Eq. (12) forces the system to increase its period of vibrations five times. For $n = 4, 5, 6$, chaos associated with fundamental frequency is produced. To sum up, similarly to the case of constant thickness shell, beginning from $n = 4$, one may observe a convergent averaged sequence exhibited by the power spectrum. Based on the previous discussion, one may conclude that variation of shell's thickness does not influence the convergence property of the Ritz method.

5. Spherical Shells with Non-Homogeneous Thickness

Although turbulence has been known for hundreds of years, mathematical modeling of the transition from smooth flows into chaos started with Landau's work.[28] Following this, other models were proposed by Feigenbaum,[29] Ruelle–Takens–Newhous,[30] and Pomeau–Manneville.[31] However, none of the mentioned existing models (and others known to us) can properly describe the transition from harmonic vibration to chaos in our deterministic vibrations of the spherical and conical shells with constant and changeable thickness for an arbitrary set of boundary conditions and deflection arrow values. The mentioned control parameters play an essential role in the transition to chaos owing to the change of amplitude and frequency of excitation. In what follows, we are going to study the influence of the assumed thickness change of the form $h = h_0(1 + c\rho)$ on the vibrations characteristics with respect to the boundary conditions and the shape of the shell cross-section. Let us analyze spherical shells with $k = 5$. We consider the spherical shell with moving clamped and deflection (convexity) arrow $k = 5$ constant ($c = 0$) and non-constant thickness ($c = 0.1, -0.1$).

To this end, charts were plotted in Fig. 6 for various combinations of control parameters $\{q_0, \omega_p\}$ through a computation of 400×500 points. An algorithm is used for analyzing the vibration characteristics, including the Lyapunov exponents, in terms of the control parameters $\{q_0, \omega_p\}$ from the power spectrum.

As can be seen from Fig. 6, the influence of thickness change is remarkable for low frequencies and those close to eigenfrequency of free vibration. For the shell with $c = 0.1$, the surface area of bifurcation and chaotic vibration is essentially smaller than that of constant thickness and that for $c = -0.1$. In other words, the variation of thickness has forced chaotic vibrations to transit into harmonic ones, and into a series of bifurcations. For $c = -0.1$, on the contrary, the area of chaotic vibrations increases remarkably. It is clearly visible for frequencies higher than the eigenfrequency value, namely, one may control the vibration of the mechanical system considered through the change in thickness.

It was reported[24] that for a shell with constant thickness after harmonic vibrations with the excitation frequency, a further increase of q_0 excites a new linearly independent frequency, and a transition to chaos is associated with the series of linear combinations of these two frequencies and Hopf bifurcations. However, the aforementioned scenario does not appear for $h(\rho) = (1 + c\rho)$, where $c \geq 0.2$. Contrary to $c < 0.2$, for the considered case, a linear combination of two independent frequencies does not lead to chaos or "stiff" stability loss. Rather, the system exhibits harmonic vibrations. Let us analyze this scenario in some detail using the example of the shell with a varying frequency of the form $h(\rho) = (1 + c\rho)$, where $c = 0.2$. The vibration characteristics considered are: signal $w(0, t)$, phase portrait $w(\dot{w})$, power spectrum $S(\omega_p)$, Poincaré section $w(w(t+T))$. In Table 3, for simplicity, the following notation is used: $w_i = w(t)$, $w_{i+1} = w(t+T)$, where T is the period of excitation, and the vibration characteristics are expressed in the threshold value

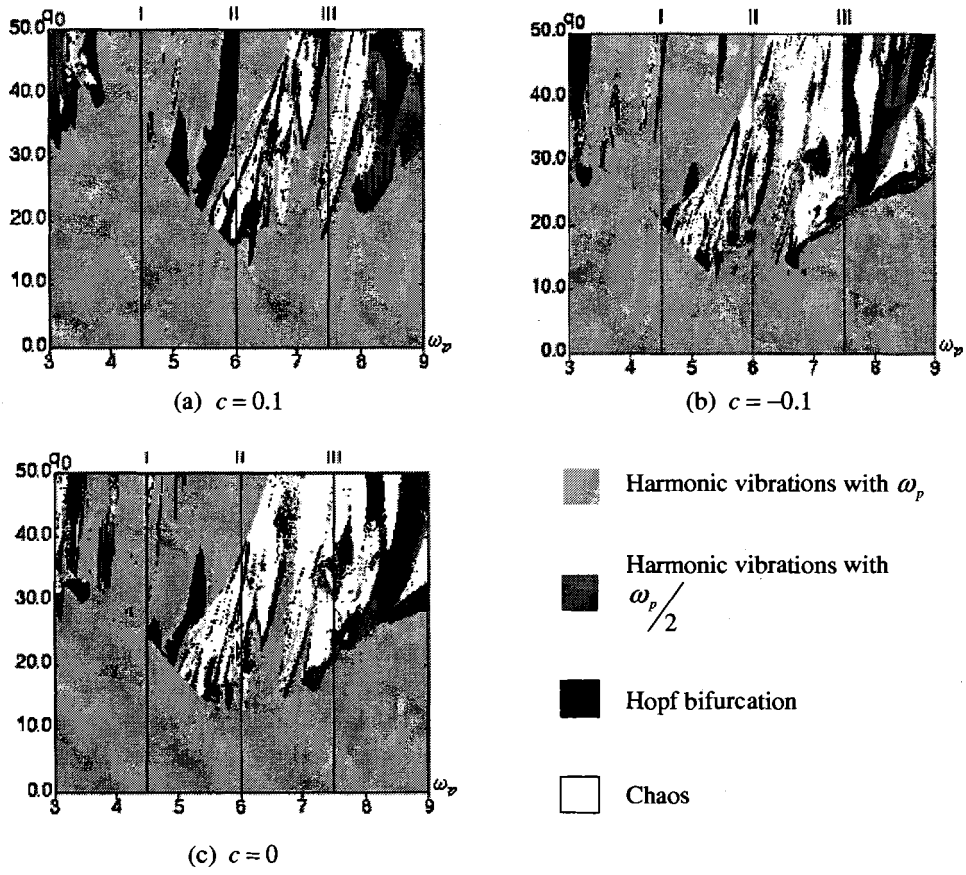

Fig. 6. Vibrational charts in terms of the control parameters $\{q_0, \omega_p\}$ for spherical shells for $k = 5$ (moving damping).

of q_0, in the sense that between successive threshold values of q_0 a picture remains practically unchanged. The following is the behavior observed from Table 3:

1. Vibrations which occur on the fundamental excitation frequency a_1 are harmonic. Phase portrait represents a manifold of one rotational cycle ($q_0 = 15$).
2. Further increase of q_0 up to $q_0 = 15.9$ causes an occurrence of the second independent frequency b_1, i.e. two-frequency motion with frequencies a_1 and b_1 is observed. The occurring motion is not synchronized because $\frac{a_1}{b_1} = \frac{m}{n} = 8.859...$ is an irrational value.
3. The increase of q_0 up to $q_0 = 16$ causes the occurrence of the series of linearly dependent frequencies $b_n = n \cdot b_1$ and $a_n = a_1 - (n-1)b_1$. The mentioned process continues until the frequencies approach each other, i.e. a_k, $b_k \in [b_1, a_1]$.
4. For $q_0 = 16.4$, period doubling associated with the frequency b_1 occurs, i.e. Hopf bifurcation takes place.

Table 3. Signals, phase portraits, power spectra and Poincaré sections.

q_0	Signal $w(0,t)$	Phase portrait $w(\dot{w})$	Power spectrum $S(\omega_p)$	Poincaré section $w(w(t+T))$
15.	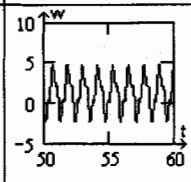	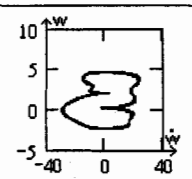	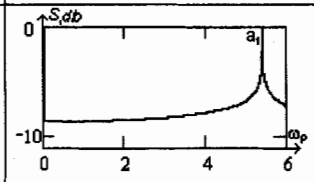	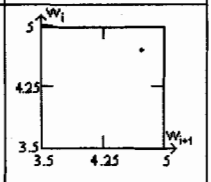
15.9	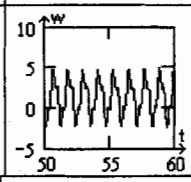	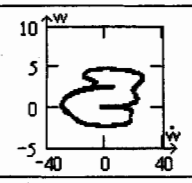	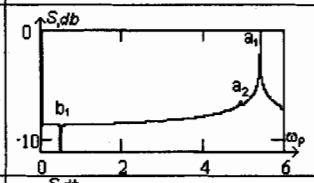	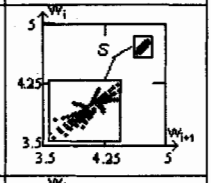
16.	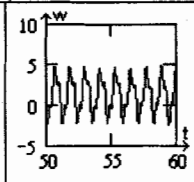	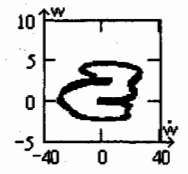	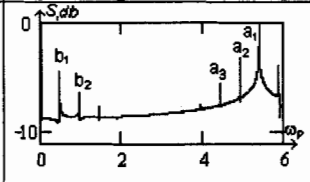	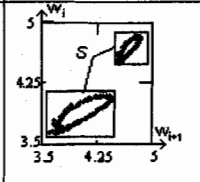
16.4	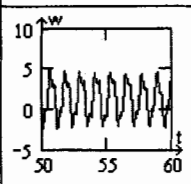	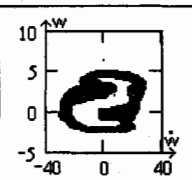	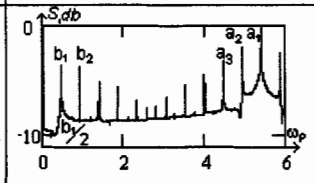	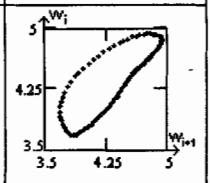
17.	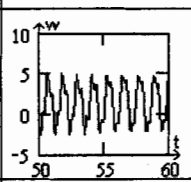	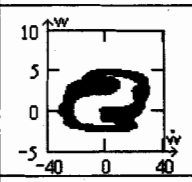	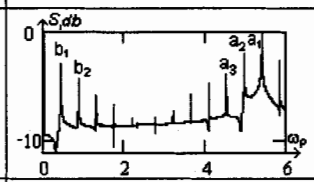	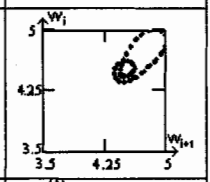
17.5	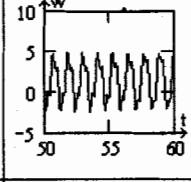	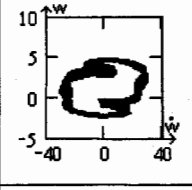	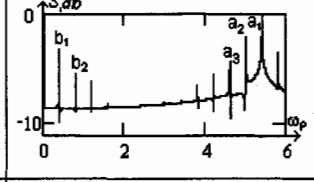	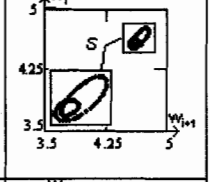
17.7	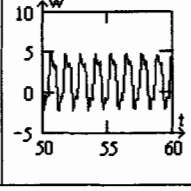	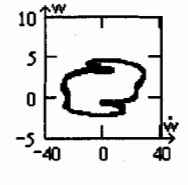	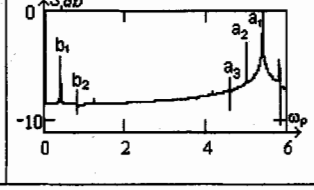	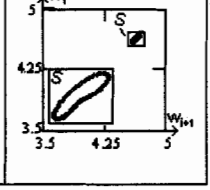

Table 3. (*Continued*)

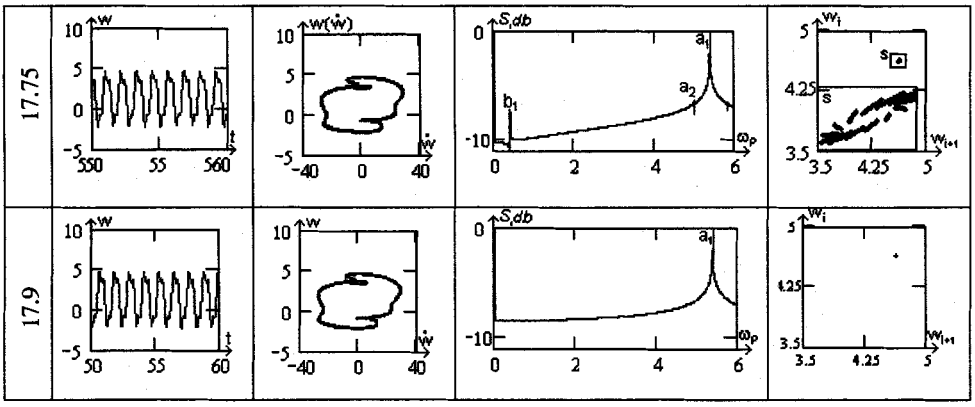

5. Further, the number of frequencies in linear combination decreases to only two independent ones ($q_0 = 17.8$).
6. For $q_0 = 17.9$, a collapse of the torus occurs, and only one frequency a_1 remains.

From the above discussion, it is clear that the "stiff" stability loss and chaos do not occur for the case considered. In other words, owing to an appropriate variation of the shell thickness one can avoid chaotic vibrations and "stiff" stability loss of the shell. Such an observation seems to have an important meaning in applications.

6. Chaotic Vibrations of Conical Shells with Non-homogeneous Thickness

Consider a shallow conical shell with constant and non-constant thickness: $h = (1+c\rho)$, with clamped moveable and ball-type movable support. They are treated as plates with initial deflection $w_0 = -k(1-\rho)$, where $k = H/h_o$ denotes a deflection arrow of the shell. The boundary conditions can be approximated by the following functions:

(i) movable ball-type support

$$w_i(\rho) = (1-\rho^2)^i, \quad \varphi_j(\rho) = (1-\rho^2)^{i+1}, \tag{22}$$

(ii) movable clamping support

$$w_i(\rho) = (1-\rho^2)^{i+1}, \quad \varphi_j(\rho) = (1-\rho^2)^{i+1}. \tag{23}$$

The applied loading $q = q_0 \sin \omega_p t$ and the initial conditions are equal to zero.

In Fig. 7, vibrational charts were plotted in terms of the control parameters $\{q_0, \omega_p\}$ for conical moveably supported shell with deflection arrow $k = 5$ of constant ($c = 0$) and variated thickness ($c = 0.1$, -0.1). Notice that we have changed the algorithm of chart construction in order to exhibit zones of independent frequencies.

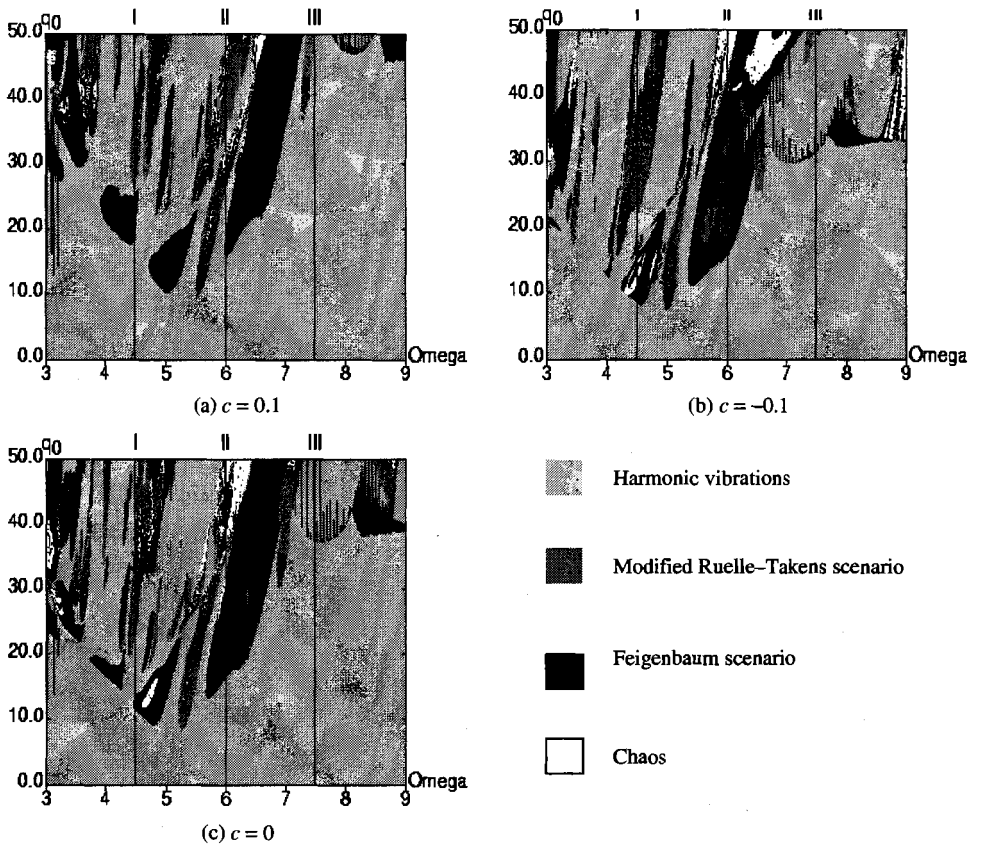

Fig. 7. Vibrational charts in terms of the control parameter $\{q_0, \omega_p\}$ for conical shells for $k = 5$ (movable clamping).

As can be seen from Fig. 7, at the shell center ($c = -0.1$), now zones of chaos occur. They are associated with high frequencies, as well as frequencies close to the free vibration frequency for the exciting amplitude $q_0 > 35$. Contrariwise, for $c = 0.1$, both the chaotic and bifurcation zones decrease.

Consider a conical shell that is moveably ball-type supported with non-constant thickness. In Fig. 8, the vibration charts in terms of the control parameters $\{q_0, \omega_p\}$ for constant and non-constant thickness for $c = 0.1, -0.1, 0.2$ for the shell with $k = 5$ were plotted. The same notation as that for Fig. 7 holds. In this case, the influence of thickness variation on the system dynamics is different from the one previously considered. For $c = -0.1$, a chaotic zone with low frequencies (about 2.5) occurs, which does not exist for $c = 0.1$, $c = 0.2$ and $c = 0$. A chaotic zone associated with high (about 5.5) frequencies exists for $c = 0$, but it does not exist for $c = 0.1$, 0.2. Contrariwise, for $c = -0.1$, on frequencies close to the eigenfrequency of vibration (≈ 3.5), the area of chaotic (harmonic) zones becomes smaller (larger) than those for other values of the parameter c. To conclude, the influence of shell thickness

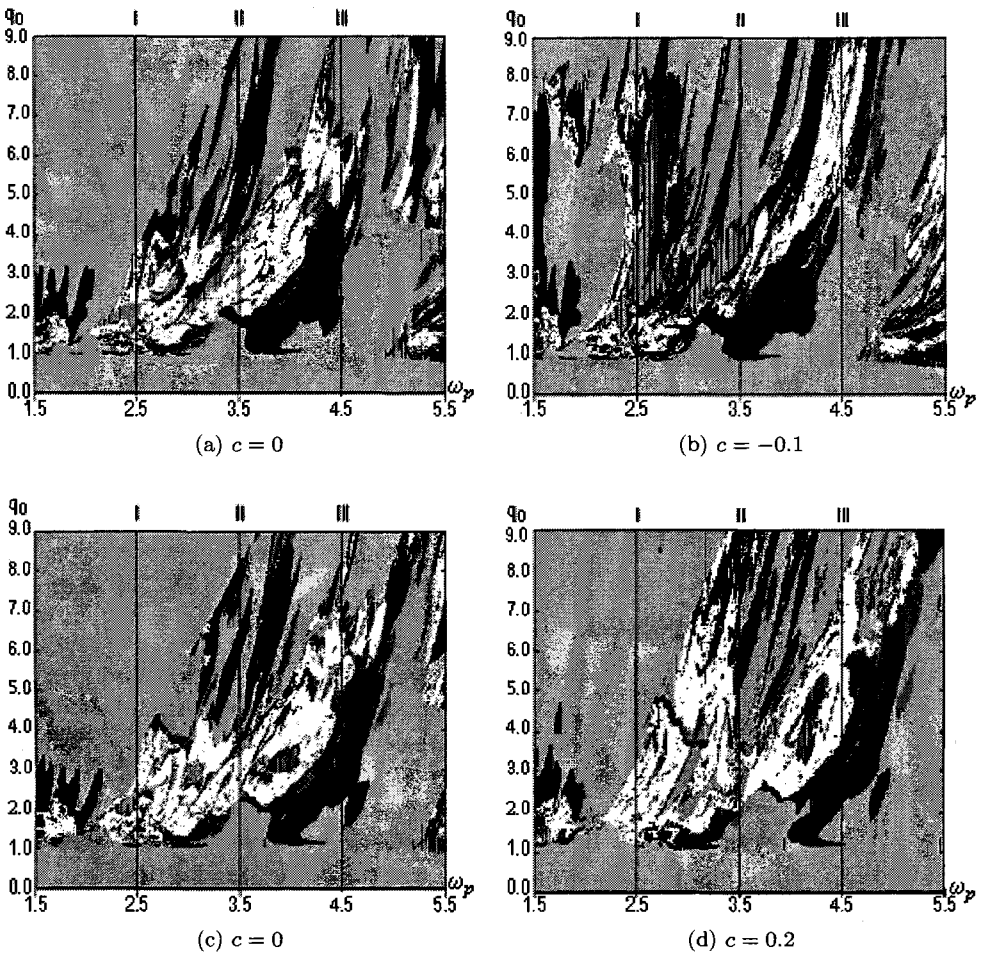

(a) $c = 0$ (b) $c = -0.1$

(c) $c = 0$ (d) $c = 0.2$

Fig. 8. Vibrational charts in terms of the control parameters $\{q_0, \omega_p\}$ for conical shell for $k = 5$ (movable ball-type support).

variations depends essentially on the geometry and boundary conditions of the shell. Thus, the vibrations of the mechanical system considered may be controlled by changing shell's cross-section, boundary conditions and load parameters q_0 and ω_p.

For the case of ball-type supported shells, an interesting behavior of signal intermittency has been observed. In Table 4 the same characteristics as those in Table 3 were listed, i.e. signal, phase portrait, frequency spectrum, and Poincaré map. They are associated with the conical shell with deflection arrow $k = 5$ and frequency of external excitation $\omega_p = 3.5$.

In this scenario, two-period doubling bifurcations were observed, and then intermittency behavior was detected, which pushed the system into a chaotic state. More details on this phenomenon are given below:

Table 4. Signals, phase portraits, power spectra and Poincaré sections.

q_0	Signal $w(t)$	Phase portrait $w(\dot{w})$	Power spectrum $S(\omega_p)$	Poincaré section $w(w(t+T))$
1.	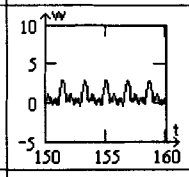	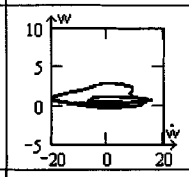	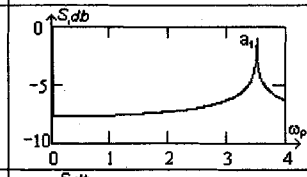	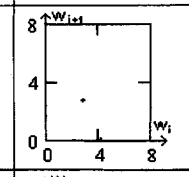
1.674	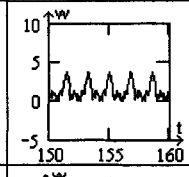	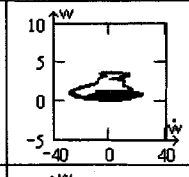	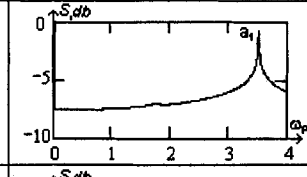	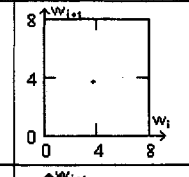
1.675	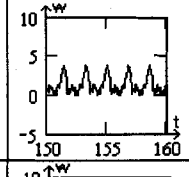	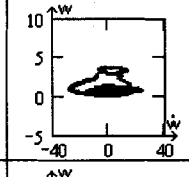	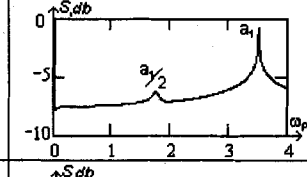	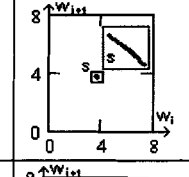
1.7	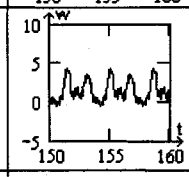	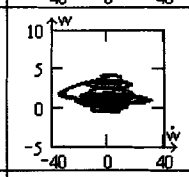	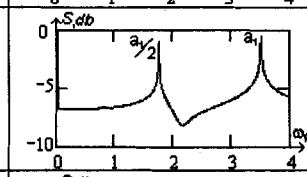	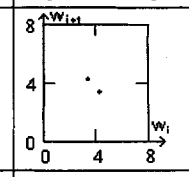
1.92	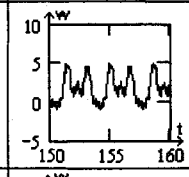	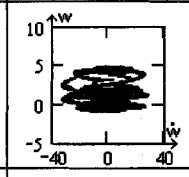	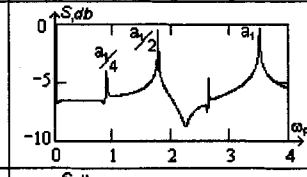	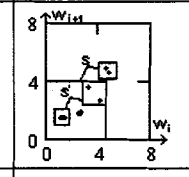
1.95	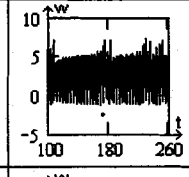	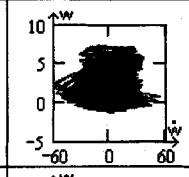	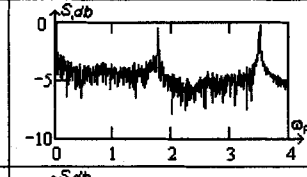	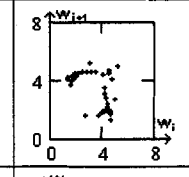
4.	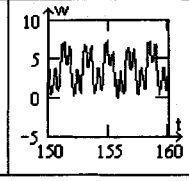	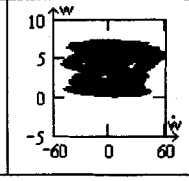	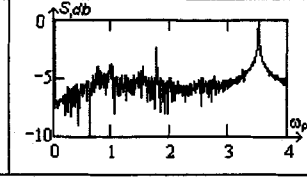	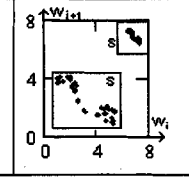

1. Vibrations associated with the frequency of excitation a_1 are harmonic ($q_0 = 1$). Phase portrait contains one rotational cycle.
2. The first soft Hopf bifurcation appears at $q_0 = 1.674$.
3. Two Hopf bifurcations occur for $q_0 = 1.92$. A loop occurs in the phase portrait.

4. Further regular parts are mixed with chaotic splashes, which increase with the increase of q_0 ($q_0 = 1.95$). This behavior is in agreement with that observed by Pomeau–Manneville and is referred to as intermittency.[31] In the power spectrum, chaos is observed already on the first Hopf bifurcation. Phase portrait successively becomes broad band.
5. In the signal, there are only few regular parts, and in the power spectrum chaos associated with excitation frequency exists.

In general, for conical ball-type movably supported shells, chaos is realized through the scenario described in Table 4. However, there are also parameter zones where follow the scenario reported in Table 3. Let us consider this scenario in a more detailed way.

In Table 5, the same characteristics as in Tables 3 and 4 for conical shells with changeable thickness (for $c = 0.1$ and with excitation frequency $\omega_p = 3.3$) were presented.

1. Vibrations associated with the fundamental excitation frequency a_1 are harmonic ($q_0 = 1.3$).
2. The increase in q_0 ($q_0 = 1.43$) results in the occurrence of a new independent frequency b_1, i.e. there is a two-frequency motion with frequencies a_1 and b_1, but not synchronized, i.e. $\frac{a_1}{b_1} = \frac{m}{n} = 2.7661....$ In the phase space two-dimensional torus is observed. The signal characteristic changes quickly. The vibrations possess relaxating property, and their impulse peaks are associated with highly energetic modes. Besides, the third independent frequency occurs, i.e. $a_2 = a_1 - b_1$. In this case the birth of a stable invariant two-dimensional torus is observed.
3. The increase of q_0 up to $q_0 = 1.45$ results in the occurrence of the series of linearly dependent frequencies $b_n = n \cdot b_1$ and $a_n = a_1 - (n-1)b_1$.
4. For $q_0 = 1.5$, the eleven time period of vibrations is observed (this behavior has been predicted by Sharkovsky's theorem[33]), and then ($q_0 = 1.7$) vibrations include again two-frequencies but with the addition of dependent frequencies of the form $c_n = a_n \pm c_2$, $c_m = b_m \pm c_2$, where $c_2 = \frac{a_4 - b_2}{2}$.
5. Further, changing q_0 up to the value of 1:8, the second independent frequency is destroyed, and a transition through one Hopf bifurcation is observed. This causes the occurrence of stiff stability loss (deflection increase sharply). Further increase of q_0 causes the occurrence of intermittent behavior which pushes the shell into a slightly developed chaotic state.

Let us analyze the Poincaré section as the amplitude of the transversal load q_0 changes. The distribution of points shows that for $q_0 = 1.45, 1.48$ there exists one attractor, which is localized in a subspace of the phase space. Its structure changes with the increase of q_0. For $q_0 = 1.7$, a chaotic motion with two fundamental frequencies and with large amount of linear combinations of these frequencies is observed. Further increase of q_0 leads to the collapse of this attractor and the birth of two attractors lying in different zones of the phase space. These attractors

Table 5. Signals, phase portraits, power spectra and Poincaré sections.

q_0	$w(t)$	Phase portrait $w(\dot{w})$	Power spectrum $S(\omega_p)$	Poincaré section $w(w(t+T))$
1.3	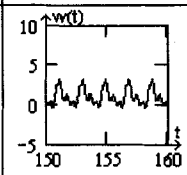	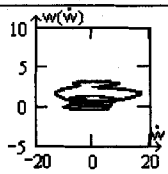	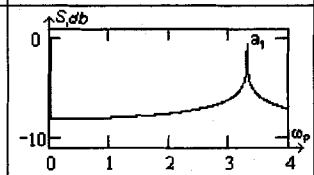	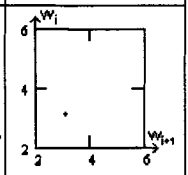
1.43	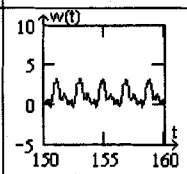	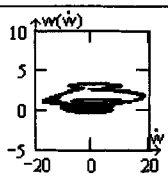	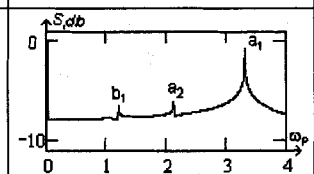	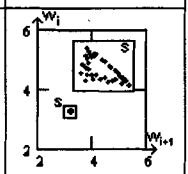
1.45	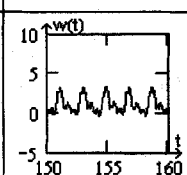	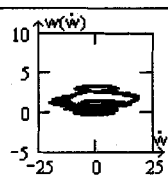	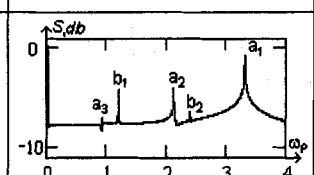	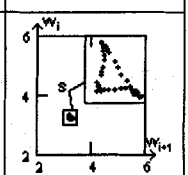
1.5	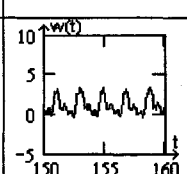	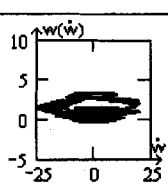	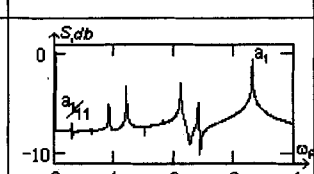	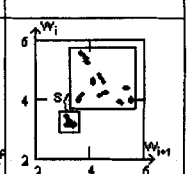
1.7	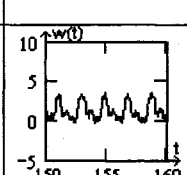	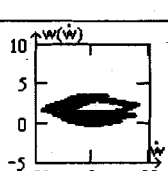	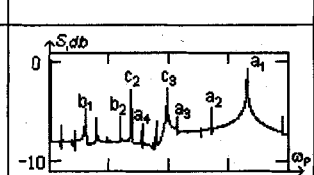	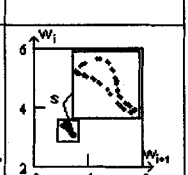
1.8	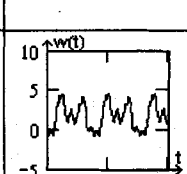	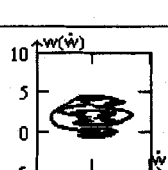	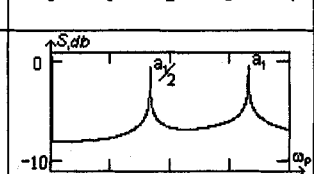	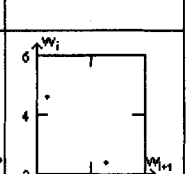

are represented by points with $q_0 = 1.8$ corresponding to one Hopf bifurcation. A slight variation of q_0 ($q_0 = 1.828$) pushes the conical shell into the chaotic regime associated with the existing frequency and first Hopf bifurcation. Attractors do not have their orbits in the phase space. The increase of q_0 to the amount of $2 \cdot 10^{-3}$

Table 5. (*Continued*)

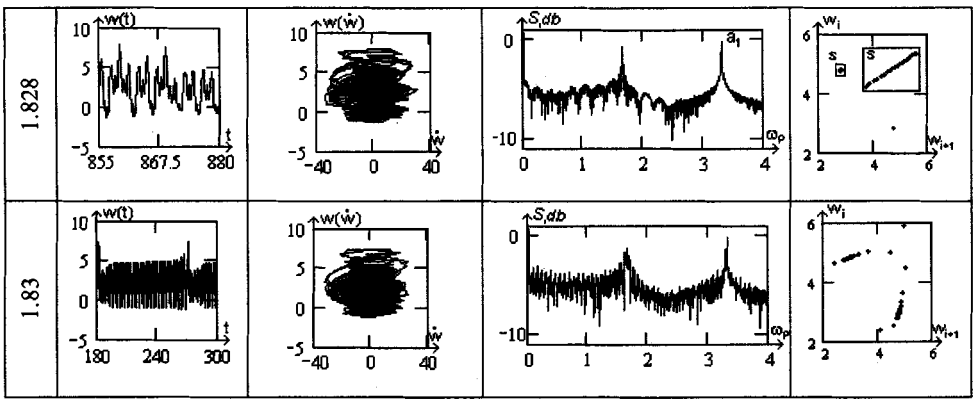

($q_0 = 1.83$) causes the occurrence of interaction between attractors. Their collapse and matching appears, i.e. one attractor is merged into the other. Besides, owing to the birth of this common attractor, matching of attracting zones of previous attractors also appears. A detailed study of this new common attractor shows that it permanently changes its position in the phase space, returning in the periodic-like manner to the initial attractors' places in the phase space. In such a process, one observes the turbulent splashes ($q_0 = 1.828$ and $q_0 = 1.832$) in $w(t)$.

In order to study the vibrations of conical shells in relation to the parameter q_0, the dependence $w_{\max}(q_0)$ and scales of the vibrational characters will be constructed. Some phenomena as those for Figs. 7 and 8 hold. In Fig. 9, these characteristics are presented for the shell's top for deflection arrow $k = 5$ for $c = 0, 0.1, -0.1$, and for shell vibrations ($\omega_p = 3.5$, 3.57 and 3.38 respectively). The first stability loss occurs for $w_{\max}(q_0)$ $q_0 = 1$. In the vicinity of $q_0 = 2$, a zone corresponding to the second stiff stability loss appears. For both critical loads, the shell with non-homogeneous thickness and with $c = 0.1$ possesses larger critical loads, whereas for $c = -0.1$ the critical loads are smaller, and the amount of a splash is smaller than that for the previous case. Also, for $c = -0.1$, the phenomenon of convexity, but not concavity, was detected, and the graph is smoother than for $c = 0, 0.1$. Conical loads for constant thickness are found in the mentioned interval. The first critical load is associated with both the first Hopf bifurcation $c = -0.1$ and second independent frequency (for $c = 0$, 0.1), which are marked in scales by the vertical lines. On bifurcation scales we observe that a chaotic zone is smaller for $c = -0.1$, which is in a good agreement with the charts shown in Fig. 8.

In what follows, we are going to investigate the occurrence of spatial-temporal chaos for the described scenario. Figures 10 and 11 show both the signal $w(0.5, t)$ and deflection of the mean shell surface for some time instants for harmonic and chaotic vibrations, respectively, for $k = 5$ and $\omega_p = 3.3$. Besides, there are given dependencies $w(\rho, t)$ for $t \in [151; 154.5]$ (Fig. 10(a)), $t \in [167.5; 169]$

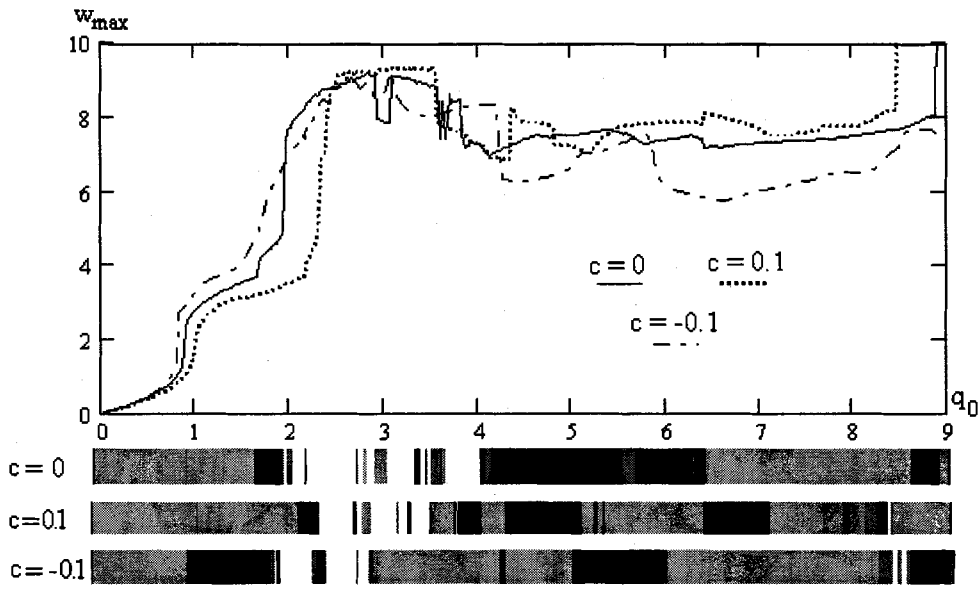

Fig. 9. Dependencies $w_{\max}(q_0)$ of conical movably ball-type supported shell with $k = 5$ for constant ($c = 0$) and variated ($c = 0.1, -0.1$) thickness.

(Fig. 11(a)). In addition, the phase portrait in space (Figs. 10(e), 11(e)), modal portrait (Figs. 10(g), 11(g)), and power spectrum (Figs. 10(h), 11(h)) ($\rho = 0.5$) were given. Simultaneous consideration of the mentioned factors allows us to analyze the signal in the spatial-temporal plane. The number of points in Figs. 10(b) and 11(b) correspond to the associated curves shown in Figs. 10(c)–(e), and Figs. 11(c)–(e). We are going to analyze the vibrations of deflection in time, separately for harmonic and chaotic vibrations. Curve 1 in Fig 10(b) characterizes the maximal deflection of the central shell point, and the quadrants are left below (Fig. 10(c)). Owing to the shell center movement down on the curve $w(t)$, points 2 and 3 are obtained in Fig. 10(b). The shell center moves down, whereas the shell quadrants start to move up (curves 2 and 3 in Fig. 10(c)). Further, harmonic vibrations around the neutral equilibrium state take place (curves 4–9 in Figs. 10(d), (e)).

Qualitatively, a similar picture is observed in Fig. 11, but the number of halfwaves appears to be higher (Figs. 11(d), (e)).

In order to have a picture of the system change in time, the following characteristics are required: signal $w(t)$, its velocity $\dot{w}(t)$ and acceleration $\ddot{w}(t)$. Let us construct the graph of the function $f(w, \dot{w}, \ddot{w})$, which will be further called a three-dimensional phase portrait. Analogously, in order to study the bending characteristics of the deflection function $w(t, \rho)$, the angle of the tangent slope $w'_\rho(t, \rho)$ and the surface curvature $w''_{\rho\rho}(t, \rho)$ are constructed for the point ρ. The mentioned set of functions allows us to study the space state of the shell surface, as well as to analyze the transition of the mechanical system from harmonic to chaotic vibrations. The

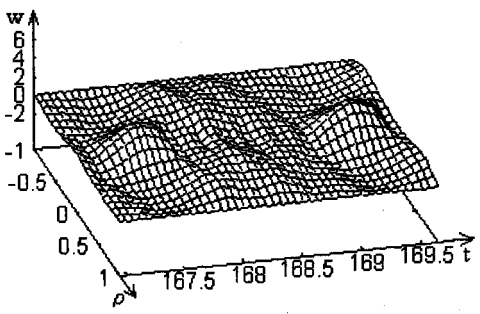

(a) $w(t,\rho), t \in [166;170]$

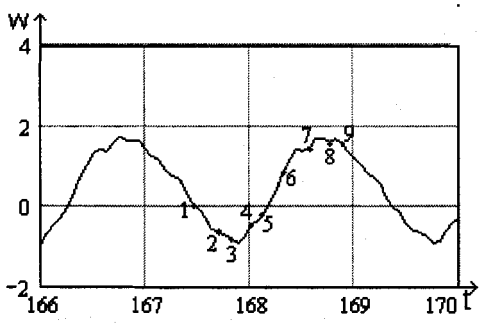

(b) $w(t,\rho), t \in [166;170]$

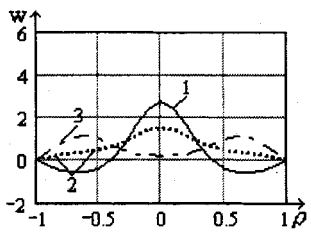

(c)

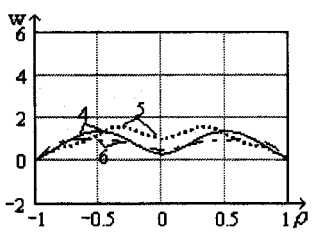

(d)

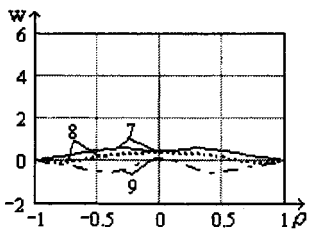

(e)

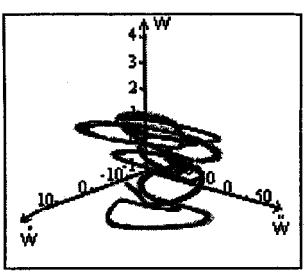

(f) phase portrait

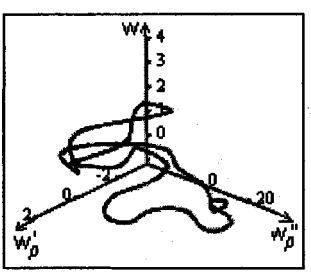

(g) model portrait

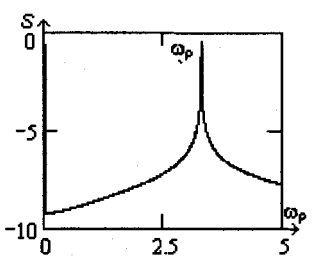

(h) power spectrum

Fig. 10. Spatial-temporal characteristics of the system behavior in harmonic vibrations regime.

dependence $f(w, w'_\rho, w''_{\rho\rho})$ is called the modal portrait. In the following, the phase and modal portrait of harmonic and chaotic vibrations is studied.

Figures 10(f) and 10(g) show that the phase and modal portraits represent one rotational cycle of vibrations in the space. Figures 11(f) and 11(g) show the phase and modal portraits for the system in a chaotic state. Both graphs represent a structure typical for chaotic vibrations. This discussion leads to the conclusion that spatial and temporal chaos appear simultaneously.

7. Conclusions

We have proposed an approach for investigating the chaotic vibrations of elastic shallow spherical and conical shells with non-homogenous thickness in relation to

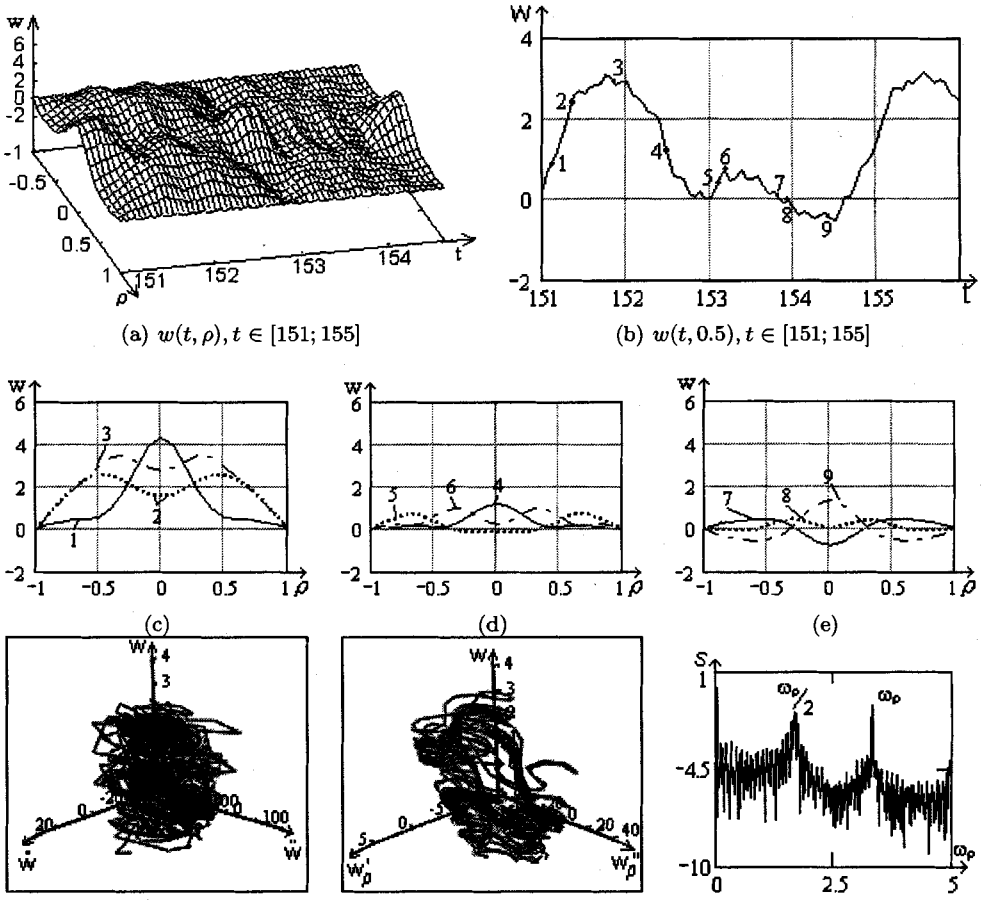

(a) $w(t,\rho), t \in [151;155]$ (b) $w(t,0.5), t \in [151;155]$

(f) phase portrait (g) model portrait (h) power spectrum

Fig. 11. Spatio-temporal characteristics of the system in a chaotic regime.

both the amplitude and frequency of the exciting transversal load. Vibration charts are plotted for conical and spherical shells with variated thickness in terms of the control parameter $\{q_0, \omega_p\}$ for two types of boundary conditions. The influence of shell thickness variation, as well as the shape of transversal shell cross-section and boundary conditions, have been studied. In addition, the question of chaos control through shell thickness adjustment has been addressed. A novel scenario of transition from harmonic to chaotic vibrations for the spherical and movably supported shells has been detected. It is associated with the occurrence of a second independent frequency and the series of linear combinations with the excitation frequency, which has been referred as the modified Ruell–Takens scenario.

Secondly, a novel scenario transition from harmonic to chaotic vibrations for movably-ball-type supported conical shells with variated thickness has been detected. It is associated with intermittency and a new scenario of matching of

intermittency and non-dependent frequencies. Spatial chaos and its interaction with temporal chaos have also been illustrated.

References

1. W. Ritz, Über eine neue Methode zur Lösung gewisser Variationsprobleme der mathematischen Physik, *J. Reine Angew. Math.* **135** (1908) 1–61.
2. S. G. Mikhlin, *Variational Methods in Mathematical Physics* (Nauka, Moscow, 1970) (in Russian).
3. S. G. Mikhlin, *Numerical Realization of Variational Methods* (Nauka, Moscow, 1966) (in Russian).
4. L. N. Dovbysh, Stability of Ritz method for problems of spherical theory of operators, in *Proc. Steklov's Mathematical Institute* 84 (1965) (in Russian).
5. L. N. Dovbysh and S. G. Mikhlin, On solvability of nonlinear Ritz systems, *Doklady Akademii Nauk* **138**(2) (1961) 258–260 (in Russian).
6. B. Ya. Kantor, *Nonlinear Problems of Theory of Nonhomogeneous Shallow Shells* (Naukova Dumka, Kiev, 1971) (in Russian).
7. L. Ya. Ainola, Variational problems in nonlinear theory of elastic shells, *PMM* (1957) (in Russian).
8. K. Z. Galimov, Application of variational principle of possible variation of stress-strain in nonlinear theory of shallow shells, *Izviestia VUZ*, Mathematics **1** (1958) (in Russian).
9. Kh. M. Mushtari and K. Z. Galimov, *Nonlinear Theory of Elastic Shells* (Tatknigizdat, Kazan, 1957) (in Russian).
10. E. Reissner, On a variational theorem in elasticity, *J. Math. Phys.* **29** (1950) 90–95.
11. I. I. Vorovich, *Mathematical Problems of Nonlinear Theory of Shallow Shells* (Moscow, Nauka, 1989) (in Russian).
12. V. I. Fedos'ev, On one method of solution of stability of deformable systems, *PMM* **27**(2) (1963) 265–275 (in Russian).
13. J. Awrejcewicz, V. A. Krysko, *Nonclassical Thermoelastic Problems in Nonlinear Dynamics of Shells* (Springer-Verlag, Berlin, 2003).
14. J. Awrejcewicz, V. A. Krysko and A. V. Krysko, Regular and chaotic behaviour of flexible plates, *European Congress on Computational Methods in Applied Sciences and Engineering*, ECCOMAS Computational Fluid Dynamics Conference 2001, Swansea, Wales, UK, 4–7 September 2001, CD ROM, 9 pages.
15. J. Awrejcewicz, V. A. Krysko and A. V. Krysko, Spatial-temporal chaos and solitons exhibited by von Kármán model, *Int. J. Bifur. Chaos* **12**(7) (2002) 1465–1513.
16. V. A. Krys'ko, G. G. Narkaitis and J. Awrejcewicz, Bifurcations of thin plates transversally and sinusoidally excited, in *Proc. 4th International Conference on Structural Dynamics* EURODYN 2002, eds. H. Grundmann and G. I. Schuëller, Munich, Germany, September 2–5 (2002), pp. 529–534.
17. J. Awrejcewicz and V. A. Krysko, Feigenbaum scenario exhibited by thin plate dynamics, *Nonlin. Dynam.* **24** (2001) 373–398.
18. V. A. Krysko, A. A. Copenko and E. V. Saliy, Complex vibrations of geometrically and physically nonlinear rectangular shallow shells, *Izviestia VUZ, Appl. Nonlin. Dynam.* 1–2 (2002) 92–103 (in Russian).
19. J. Awrejcewicz and A. V. Krysko, Analysis of complex parametric vibrations of plates and shells using Bubnov–Galerkin approach, *Arch. Appl. Mech.* **73** (2003) 495–504.
20. J. Awrejcewicz, V. A. Krysko and A. V. Krysko, Complex parametric vibrations of flexible rectangular plates, *Meccanica* **39**(3) (2004) 221–244.

21. J. Awrejcewicz, V. A. Krysko and A. Vakakis, *Nonlinear Dynamics of Continuous Elastic Systems* (Springer-Verlag, Berlin, 2004).
22. V. V. Novozhilov, *Fundamentals of Nonlinear Theory of Elasticity* (Gostekhizdat, Moscow, 1948) (in Russian).
23. A. S. Volmir, *Stability of Deformable Systems* (Nauka, Moscow, 1967) (in Russian).
24. V. A. Krysko and T. V. Shchekaturova, Chaotic vibrations of conical shells, *Izviestia RAW Rigid Body Mechanics (Mekhanika Tviordogo Tela)* **5** (2004) 153–163 (in Russian).
25. E. N. Lorenz, Deterministic nonperiodic flow, *J. Atmos. Sci.* **20**(2) (1962) 130–148.
26. J. H. Curry, J. R. Herring, J. Loncaric and S. A. Orszag, Order disorder of two- and three-dimensional Benard convection, *J. Fluid Mech.* **147**(1) (1984) 1–38.
27. J. Awrejcewicz and V. A. Krysko, Nonlinear coupled problems in dynamics of shells, *Int. J. Eng. Sci.* **41**(6) (2003) 587–607.
28. L. D. Landau, To the problem of turbulence, *DAN SSSR* **44** (1944) 339–344.
29. M. J. Feigenbaum, The universal metric properties of nonlinear transformations, *J. Stat. Phys.* **21**(6) (1979) 669–706.
30. D. Ruelle and F. Takens, On the nature of turbulence, *Commun. Math. Phys.* **20** (1974) 167–192.
31. P. Manneville and Y. Pomeau, Different ways to turbulence in dissipative dynamical systems, *Physica* **D1** (1980) 219–226.
32. V. A. Krysko and A. V. Krysko, Bifurcations and stiff stability loss in nonlinear theory of plates, Mechanics of shells and plates in XXI century, Saratov (Saratov State University Press, 2003), pp. 50–67 (in Russian).
33. A. N. Sharkovskiy, Coexistence of cycles of a continuous map of a linear into itself, *Ukr. Math. Z.* **16**(1) (1964) 61–71 (in Russian).